Journal of Applied Polymer Science

In-situ grown silica/water-borne epoxy shape memory composite foams prepared without blowing agent addition

Yubing Dong,[1] Yaqin Fu,[2] Qing-Qing Ni[1,2]

[1]Department of Functional Machinery and Mechanics, Faculty of Textile Science and Technology, Shinshu University, 3-15-1 Tokida, Ueda 386-8576, Japan

[2]Key Laboratory of Advanced Textile Materials and Manufacturing Technology Ministry of Education, Zhejiang Sci-Tech University, Hangzhou, Zhejiang 310018, China

Correspondence to: Q.-Q. Ni (E-mail: niqq@shinshu-u.ac.jp.)

ABSTRACT: Shape memory (SM) silica/epoxy composite foams were successfully synthesized via latex technology and prepared without blowing agent addition. Silica was synthesized via tetraethoxysilane (TEOS) hydrolysis. Silica/epoxy foams were obtained from the TEOS solution and water-borne epoxy mixtures after freeze-drying and foaming in the presence of residual moisture as the blowing agent under a vacuum at 110°C. The morphologies of the resulting foams were evaluated using scanning electron microscopy (SEM) and transmission electron microscopy (TEM). Compression and thermo-mechanical cycle tests were performed to measure the mechanical and SM properties of the foams. Experimental results indicated that the micrographs and mechanical properties of the foams were closely related to freeze-drying time. The final composite foams exhibited high shape recovery and fixity ratios and could maintain both properties at more than 90% even after five thermo-mechanical cycles. The properties obtained in the epoxy foams may offer new opportunities for their use in future structural applications. © 2015 Wiley Periodicals, Inc. J. Appl. Polym. Sci. **2015**, *132*, 42599.

KEYWORDS: colloids; composites; foams; functionalization of polymers; synthesis and processing

Received 15 March 2015; accepted 10 June 2015
DOI: 10.1002/app.42599

INTRODUCTION

Shape memory polymers (SMPs) can be fixed into a stable temporary shape, and then revert to their permanent shape when triggered by external stimuli.[1–4] These stimuli, include heat,[5,6] water,[7] pH,[8] light,[9] electricity,[10,11] and magnetic fields.[12,13] Increasingly demanding industry requirements in terms of developing polymer-based foams with shape memory (SM) properties have recently attracted considerable interest worldwide.[1–3] Compared with fully dense SMPs, SMP foams possess lower density, and higher compressibility, can achieve higher temporary deformations and exhibit higher deformations when they recover their permanent shape. Thus, SMP foams have the potential use in a wide range of applications, such as biomedical devices,[14] aerospace structures,[15] and self-healing applications.[16]

Thermo-responsive SMP foams, are commonly categorized into polyurethane-based,[17,18] polystyrene-based,[19,20] and epoxy-based foams.[21–23] SM epoxy foam has superior environmental durability, and is a good candidate for space application. However, the processes involved in developing epoxy foam are environmentally unfriendly, complex, and expensive. A vast majority of the foam products are still formulated with organic blowing agents, such as, azodicarbonamide,[24] p,p′-oxybis(benzene sulfonyl hydrazide),[25] and supercritical carbon dioxide.[26,27] However, as environmental regulation becomes stricter, the requirement for the industries to switch to more ecological and safer systems is constantly increasing.

Our previous research found that environmentally friendly water-borne epoxy (WEP) has excellent SM effect.[28] However, WEP possesses an inferior mechanical strength and a lower SM fixity ratio compared with conventional solvent-based epoxies. Improvements in the mechanical and SM properties of SMPs have been achieved by incorporating inorganic particles.[29,30] Among the numerous additives, silica particles are commonly used because of their chemical stability, favorable morphology, availability, and low price. However, similar to other particles, silica is prone to cluster in the polymer and cannot obtain excellent composites because of the poor interfacial compatibility between the polymer matrix and the silica. Zhang *et al.*[31] and Lee *et al.*[32] used polycaprolactone-grafted and allylisocynate-

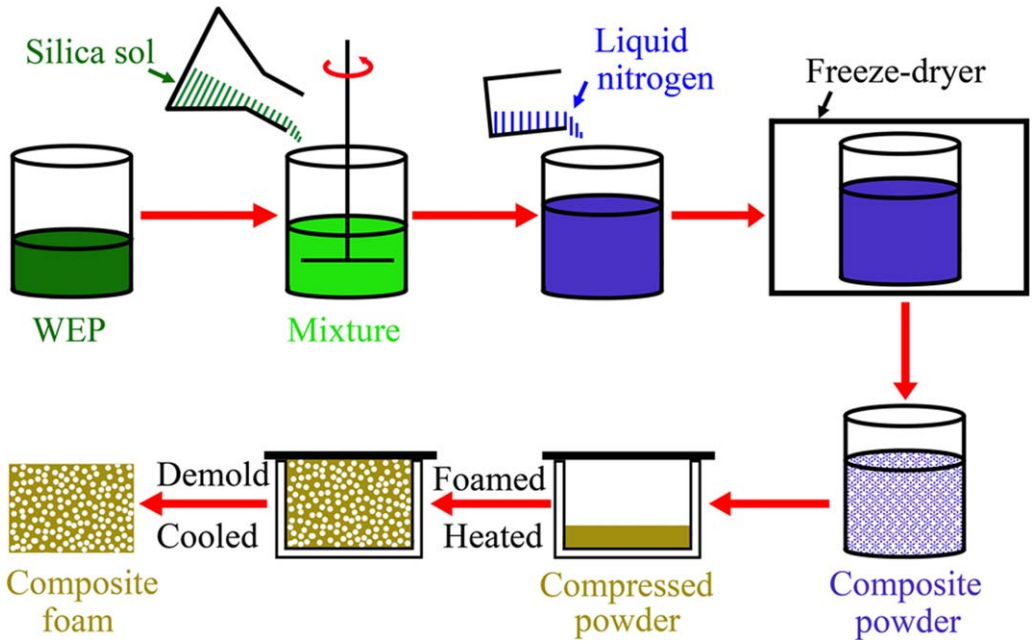

Figure 1. Schematic of the process for preparing silica/WEP foams. [Color figure can be viewed in the online issue, which is available at wileyonlinelibrary.com.]

modified silica, respectively, to improve polycaprolactone and water-borne polyurethane SM effects. The resultant silica/SMP composites exhibit excellent mechanical strength and SM properties. In the present study, an environmentally friendly method was introduced to synthesize SM silica/epoxy composite foams form WEP. The mechanical and SM properties of the silica/epoxy foams were evaluated along with other physical properties. The final composite foams exhibited high shape recovery and fixity ratios and could maintain both properties at more than 90% even after five thermo-mechanical cycles.

EXPERIMENTAL

Materials

Commercially available epoxy resin (diglycidyl ether of bisphenol A) E-44 (epoxy equivalent~213-244) was supplied by Wuxi Resin Factory, China. The emulsifier for WEP is a new reactive copolymerepoxy-toluene diisocyanate-Triton X-100 (EP-TDI-TX100), which has been successfully synthesized in our previous research.[33] Room-temperature nonionic type water-borne epoxy curing agent (AB-HGF®) was obtained from Zhejiang Anbang New Material Development, China. Tetraethoxysilane (TEOS), 3-triethoxysilylpropylamine (KH550), and absolute ethanol were acquired from commercial sources and used as received. All experiments were performed using deionized (DI) water.

Preparation of Silica/WEP Foams

First, a curing agent was initially added to the WEP and dispersed to homogeneity at room temperature by intensive mixing in a beaker at 500 rpm for 15 min. The weight ratio of the epoxy to the curing agent was 4 : 1. Subsequently, a known volume of silica sol (KH550 : TEOS : ethanol = 1 : 5 : 20, w/w/w) was poured into the WEP and curing agent mixture. Second, the resulting mixture was mixed at 1000 rpm for 15 min, and then frozen in liquid nitrogen. The aqueous solvent and ethanol were removed using a Labconco Free Zone freeze-dry operated system at 0.1 mbar and −55°C for 3, 4, and 5 days (d). The resulting powder was shaped via cold compaction in a 15 mm tall and 35 mm wide cylindrical stainless steel mold at a packing pressure of 5 MPa for a holding time of 5 min. Third, the epoxy tablets were foamed in a vacuum oven at 110°C and −0.1 MPa for 4 h and post-cured at 120°C for 12 h. Figure 1 illustrates the fabrication procedure of the silica/WEP foams.

Morphology of Silica/WEP Foams

Scanning electron microscopy (SEM) observations of the specimens before and after compression were conducted using a field emission scanning electron microscope (Ultra 55; Zeiss, Germany) at an operating voltage of 3 kV. Prior to testing, samples were sputter-coated with gold to impart electrical conductivity and reduce charging artifacts. High vacuum conditions were applied and a secondary electron detector was used for image acquisition. The average cell size and cell density of the silica/WEP foam were obtained by image analysis on the SEM images using ImageJ software. Cell density (N_f) was determined by the number of cells per unit volume of foam, which was calculated by eq. (1), where n and A are the number of bubbles and the area of the micrograph (cm^2), respectively. Transmission electron microscopy (TEM) images of the silica/WEP foams were obtained from ultrathin sections that were cut with a glass knife on the Leica EM UC7 ultramicrotome (Leica, Germany) and examined using a transmission electron microscope (JEM-2100F; JEOL, Japan) operated at 200 kV. All density measurements of the foams were performed by dividing the sample weight by the sample volume, by using an analytical balance and a caliper. Foam density was calculated on 10 mm long cylindrical

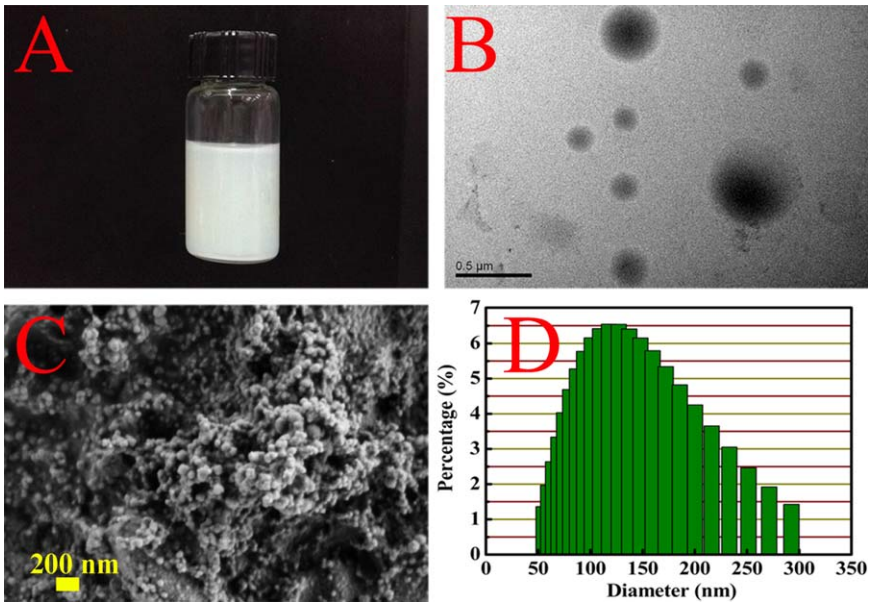

Figure 2. (A) Image of the water-borne epoxy (WEP), (B) TEM micrograph of WEP particles, (C) SEM micrograph of WEP particles, and (D) particle size distribution for the WEP. [Color figure can be viewed in the online issue, which is available at wileyonlinelibrary.com.]

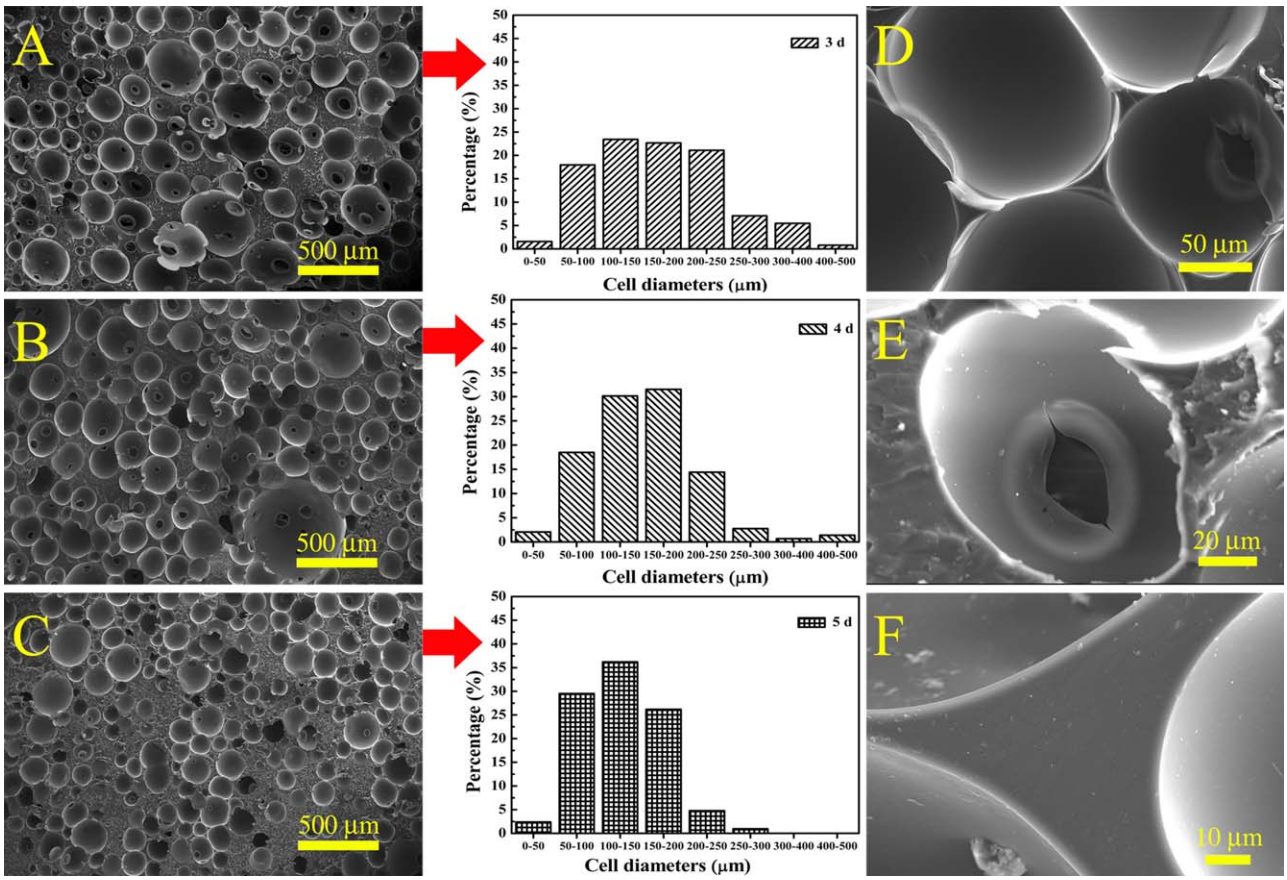

Figure 3. SEM images of silica/WEP foams and cell size distributions with different freeze-drying time: (A) SMF1 (3 d), (B) SMF2 (4 d), and (C) SMF3 (5 d). (D−F) Cell, window, and cell strut of the foam, respectively. [Color figure can be viewed in the online issue, which is available at wileyonlinelibrary.com.]

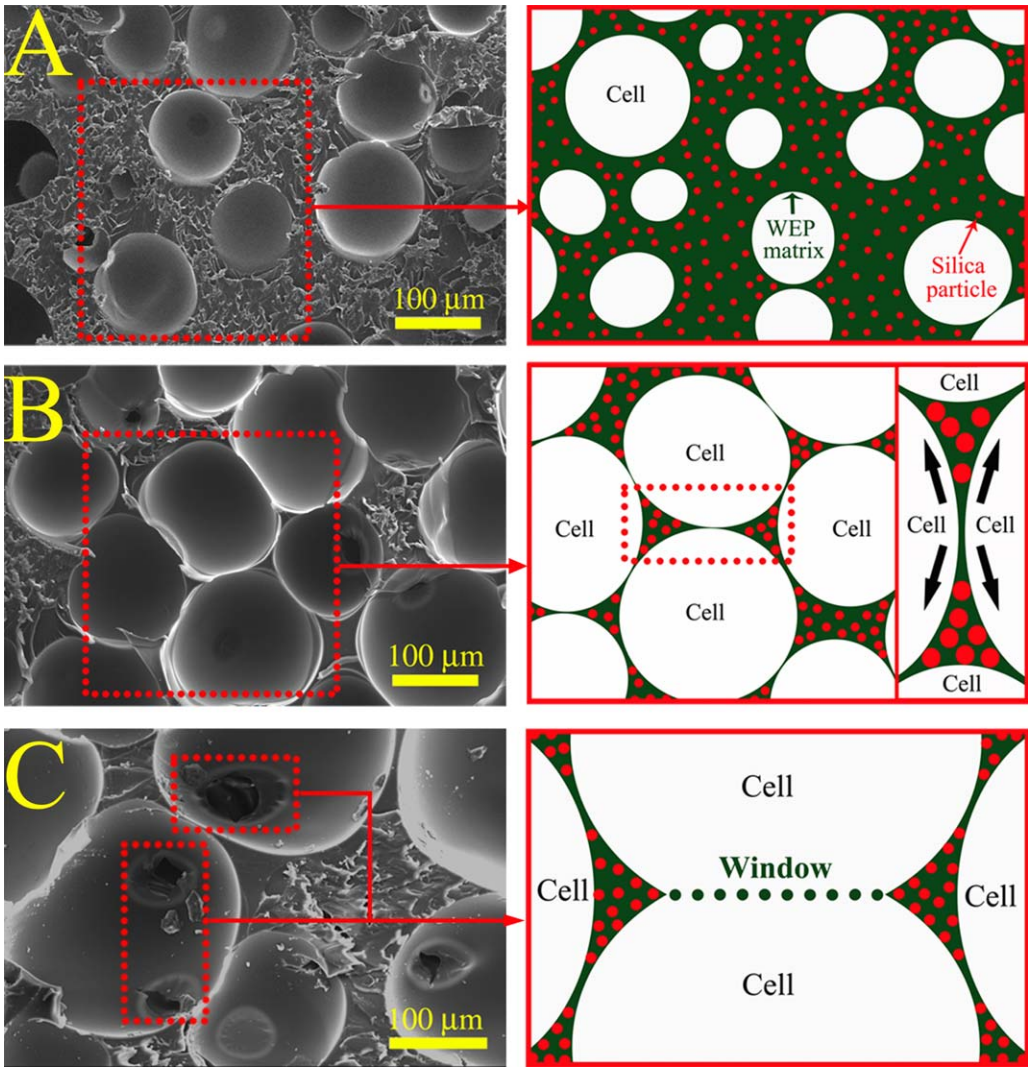

Figure 4. Foaming mechanism of the silica/WEP foam at the different stage: (A) relative density 49.1%; (B) relative density 47.4%; and (C) relative density 44.8%. The bulk density of cured WEP is 0.786 g cm^{-3}. [Color figure can be viewed in the online issue, which is available at wileyonlinelibrary.com.]

specimens extracted by sawing from the foams. The top and bottom of the foams were not considered for density measurements.

$$N_f = \left(\frac{n}{A}\right)^{3/2} \quad (1)$$

Compression Test

Compression tests were conducted flat-wise by using a universal testing machine (INSTRON 8531) to evaluate the mechanical properties of the prepared foams. The specimens were polished to a size of 10 mm × 10 mm × 25 mm and then tested. The loading rate was 1.0 mm min^{-1} at room temperature. A preload of 0.2 N was used to achieve full contact of the plate on the sample. At least five effective specimens were tested.

Dynamic Mechanical Analysis (DMA)

The thermo-mechanical properties of the foams were studied using a DMA Q800 (TA Instrument, USA). Rectangular foams with a typical dimension of 9 mm × 5 mm × 2 mm were loaded under tension and oscillatory deformation with an amplitude of 10 μm, at a frequency of 1 Hz. Samples were heated from 0°C to 100°C at a rate of 5°C min^{-1} and run under engineering strain control, with 0.1% strain and 0.01 N preload. The ends of the samples were wrapped with aluminum foil to avoid fracture in the grips.

Investigation of the SM Effect

To visually demonstrate the SM behavior, we equilibrated a rectangular foam in an isothermal oven at 55°C for 5 min to soften it well. The foam was compressed to a temporary shape and then immediately placed in a freezer at 0°C, while holding the compressive force for 5 min to fix the temporary shape. Subsequently, the already compressed specimen was heated at 55°C, and the original shape was obtained.

The SM properties of the foams were characterized with the same DMA Q800 mentioned above, but in "Force Control" mode. Cylindrical foam samples with typical dimensions of

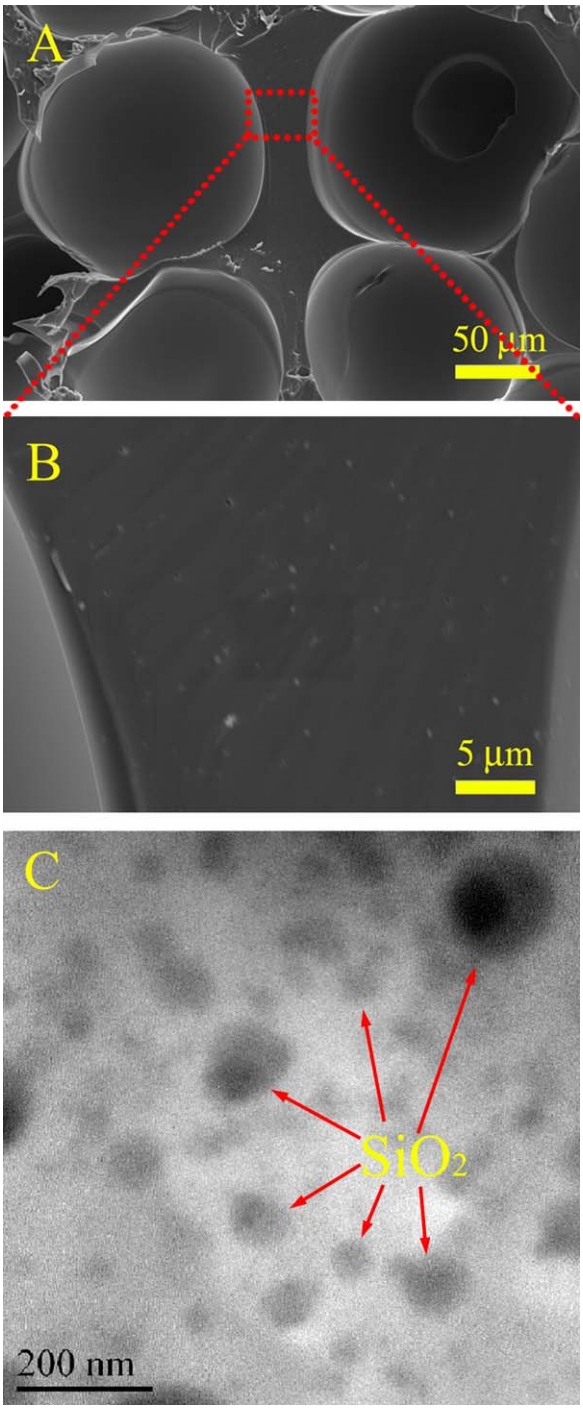

Figure 5. (A,B) SEM micrograph of silica particles in the foam cell wall, and (C) TEM micrograph of the silica/WEP foam. [Color figure can be viewed in the online issue, which is available at wileyonlinelibrary.com.]

10 mm (high) × 10 mm (diameter) were compressed to the maximum strain of 70% (ε_m) at a constant compression speed at 55°C above T_g (step 1). The specimen was cooled down to 15°C below T_g (at the glass state) and held for 10 min while maintaining the strain at 70% (step 2). The specimen was then unloaded at 15°C at a small unloading strain ε_u (step 3), completing the three-step shape fixity process. The shape recovery capacity was examined by heating the specimen from 15°C to 55°C without load and held for 10 min. The strain of the specimen was then recovered. When this cycle is finished, a residual strain remained. The heating or cooling speed was 5°C min^{-1}, and the loading and unloading speed was 1.0 mm min^{-1}. This test was repeated five times.

RESULTS AND DISCUSSION

Micrograph and Curing Mechanism of WEP

Figure 2 shows the micrograph and particle size distribution of WEP, which was synthesized from epoxy/surfactant emulsion by using the phase-inversion technique. The surfactant for the WEP is a reactive copolymer EP-TDI-TX100, which has been successfully synthesized in our previous research.[33] The mixture was then poured into a stainless steel cup and stirred at 10°C using an ice bath to maintain a low emulsification temperature. The shearing speed was 3000 rpm. DI water was then added drop-wise until phase inversion occurred. Sufficient water was added to produce a WEP with 50% solid weight. An average particle diameter of 137 nm, with particles ranging from 50 nm to 300 nm, was determined using particle size analysis (Delsa Nano C, Beckman Coulter, USA).

The WEP system is an inhomogeneous two-phase system that consists of water as continuous phase and resin emulsion droplets as dispersed phase. Water evaporates after applying WEP under atmospheric conditions. When most of the water is evaporated, the emulsion droplets come into contact and form a close pack of spheres, with the residual water (with most of the hardener dissolved in it) filling the gaps in between. Then, as the first stage of the coalescence process the emulsion droplets form hexagons before merging to a supposedly homogeneous, continuous phase. When the state of dense packing and, even more so, when the hexagonal state is reached, hardener molecules penetrate the emulsion droplets and react with the epoxy resin. Meanwhile, most of the residual water and any added coalescing solvents diffuse into the film surface and evaporate.[34] However, the curing mechanism of the WEP after freeze-drying has a slight difference from the process under atmospheric conditions. During mixing of the WEP and curing agent, the water content of the system was ~50%. When frozen in liquid nitrogen (−196°C) and freeze-dried at a low temperature of −55°C, the WEP and curing agent system was in ice form. After water in ice form sublimated, epoxy and hardener composite powder was obtained. The powder become sticky when exposed to air, because WEP is made from liquid epoxy resin, which starts to melt at room temperature. A pressure of 5 MPa was applied to pack the powder and decrease the distance between the epoxy and curing agent. In addition, the last post-curing step was performed at 120°C for 12 h to ensure curing completion. The molecular weight, viscosity and T_g of the epoxy molecules increased during the curing processing, resulting in harder droplets that are not prone to good coalescence.[35] The larger particle size of WEP makes it more difficult to obtain high curing degree in the WEP system. Therefore, the particle size and uniform distribution of WEP are two important factors that affect the WEP curing degree, which directly influence the mechanical and SM properties of the final composite foam.

Table I. Summary of Processing Conditions and Foam Parameters

Properties	SMF1	SMF2	SMF3
Freeze-drying time (d)	3	4	5
Foam density (g cm^{-3})	0.328	0.352	0.386
Average cell size (μm)	198	181	146
Cell density (cells cm^{-3})	1.67×10^5	2.03×10^5	3.35×10^5
Compressive strength at strain of 70% (MPa)	27.6	29.1	35.2
Modulus of compression (MPa)	44.3	55.2	73.9
T_g (°C)	41.5	41.6	42.0

Micrograph of the Silica/WEP Foams

Figure 3 shows representative images of cross-sectional surfaces of the silica/WEP foams with the same filler content (in previous research, the mechanical, and SM properties of WEP were significantly improved by adding silica, and the optimal mass ratio is 1.5%[6,35]). The effect of freeze-drying time on the foam morphology and cell size distribution is shown in Figure 3(A−C). The average cell sizes of the foams prepared after 3, 4, and 5 d freeze-drying were about 198.8, 181.7, and 146.8 μm, respectively. In Figure 3(A,B), windows are shown within the cells where neighboring cells met. In the higher density foam [Figure 3(C)], the average cell size is finer. Few of these windows and some unfoamed areas are also shown in the image. The phenomena can be attributed to the small amount of water (blowing agent) in ice form remaining in the composite powder and the greater amount of solid polymer available to fill between the cells because of the long freeze-drying time. Figure 3(D−F) show the cell, window, and strut of the composite foam, respectively. The cell wall thinning with decreasing density and the foaming mechanism of the silica/WEP foam at different stages are shown in Figure 4. The representative SEM image of the cell wall clearly shows the *in-situ* generated silica particles homogeneously distributed in the polymer matrix, as shown in Figure 5. The TEM image confirms the existence of the silica particles uniformly distributed and embedded in the epoxy matrix, as shown in SEM image. The silica/WEP foam parameters evaluated in the study are shown in Table I.

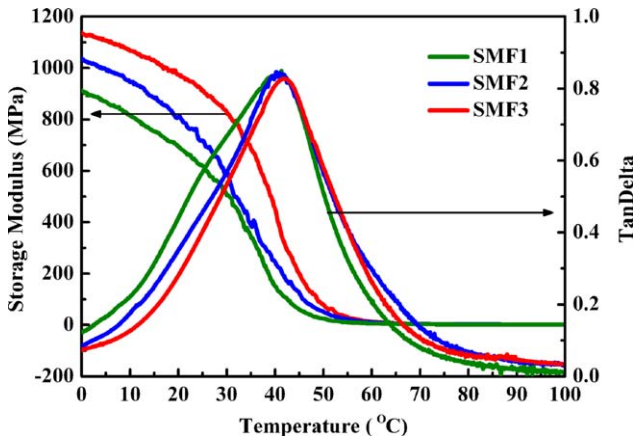

Figure 6. Storage modulus and tan delta of the silica/WEP foams from DMA testing. [Color figure can be viewed in the online issue, which is available at wileyonlinelibrary.com.]

DMA Tests

The storage modulus and tan delta values of the silica/WEP foams observed from the DMA test are shown in Figure 6. All samples underwent glass transition when the temperature was increased from 0°C to 100°C and exhibited similar temperature-dependent viscoelastic properties, as shown in Figure 6. Freeze-drying time did not significantly affect the T_g values, and as a consequence, no significant change in the cross-linking density was expected. The storage modulus observed at temperatures far below the T_g was two orders of magnitude larger than that observed at temperatures above the T_g (Figure 6). For example, the sample SMF1 exhibited storage modulus of 815.6 MPa at 10°C and 1.9 MPa at 90°C. For an excellent SMP, a large and sharp drop in the storage modulus around the glass transition is the most important.[37]

Compression Characterization

The modulus and compressive strengths of the silica/WEP foams as function of the freeze-drying time are shown in Figure 7 and Table I. The compressive stress–strain curves of the silica/WEP foams exhibited similar regimes to the stress–strain curve of regular syntactic foams. The stress–strain curve can be clearly characterized by three distinct regions, as shown in Figure 7. In the initial elastic region and during early yield, the stress almost linearly increased as the foam became rigid. Subsequently, a

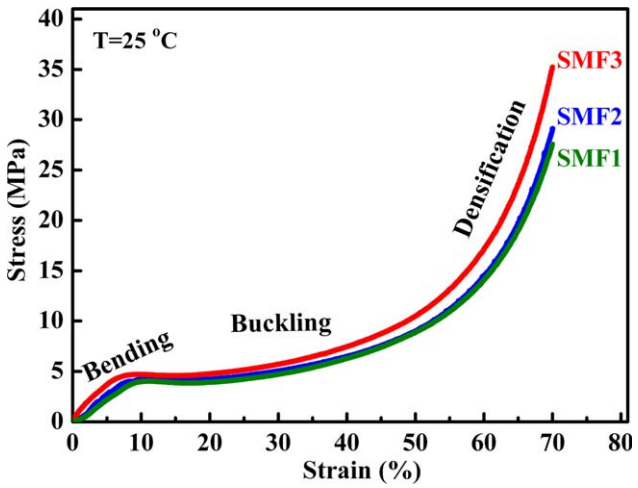

Figure 7. Compressive curve of the silica/WEP foams with different freeze-drying time: 3 d (SMF1), 4 d (SMF2), and 5 d (SMF3). [Color figure can be viewed in the online issue, which is available at wileyonlinelibrary.com.]

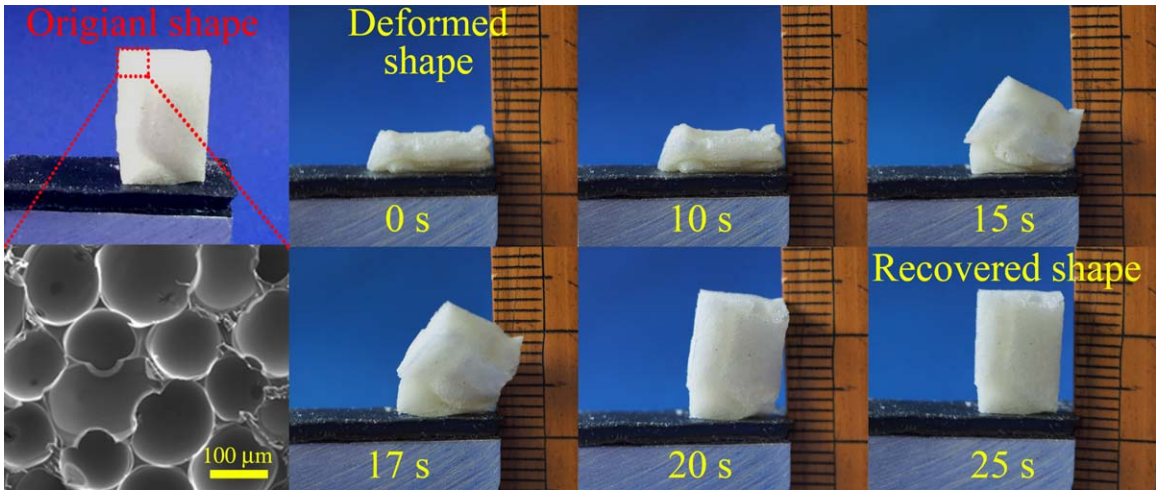

Figure 8. Series of photographs showing the macroscopic SM effect of the foam. [Color figure can be viewed in the online issue, which is available at wileyonlinelibrary.com.]

wide plateau region mainly corresponding to the rubbery and cell deformation of the foam matrix was observed. Finally, the cell collapsed and became compact with further increase in strain, and the stress–strain curve was directed upward toward higher stress, at a larger strain. Compared with regular syntactic foam, the deformation in the rubbery region was obviously higher.[21,22] This finding suggests that the foams can absorb more energy without disintegration. Notably, the mechanical properties also increased with increasing freeze-drying time. These results can be contributed to the increased in freeze-drying time, which decreased the amount of foaming agent (water), and increased the foam density. The short freeze-drying time foam (low foam density) could collapse because of the bending of the cell wall. For the long freeze-drying time foam (high foam density), the cell wall exhibited high rigidity and thickness, and depended on the matrix properties.

SM Behaviors of the Silica/WEP Foams

The shape recovery behavior of the foam is shown in Figure 8. From the shape recovery process, we found that an initial shape can be recovered in 30 s at 55°C. The foam also had the ability to undergo and recover large strains. For the thermally activated cross linked epoxy system, the SM effect is entropic in nature.[22,37] The foam was heated above the transition temperature (T_g), deformed, and subsequently cooled below T_g to fix the temporary geometry. This geometry was maintained because thermodynamic barriers prevent the polymer chains from relaxing and returning to their original state of higher entropy, which the chains automatically assumed during initial polymerization and processing. The stored energy in the material, as the configurational entropy of the chain decreased, was subsequently locked into the polymer chains, and the chains were restricted from freely rotating. After heating above T_g without constraint, an increase of entropy caused the deformed SM foam to return to its high-entropy state, which is the original geometry. At the molecular level, the covalent cross-linked netpoints of the SM foam keep the polymer chains from sliding past one another while heated above T_g.[38] Heating these foams to 55°C, deforming them to a temporary shape, and cooling to 0°C under deformation "freezes-in" the new shape and produces changes in the porous structure. Moreover, the "freezes-in" porous structures in SMF2 with compressive strains of 50% and 70% are shown in Figure 9(A,B). The voids, which are spherical in the as-synthesized SMF2, became oval on compression to the strain of 50% [Figure 9(A)]. Upon compression to the strain of

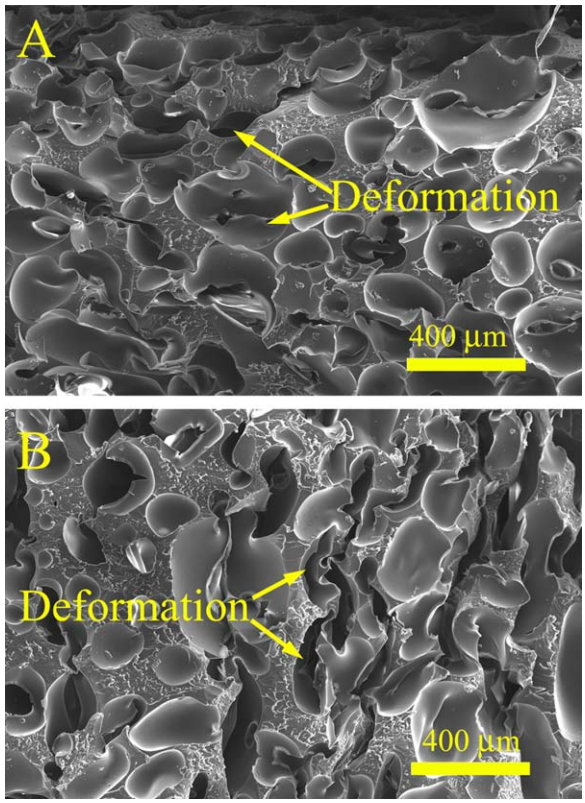

Figure 9. SEM micrographs of silica/WEP foam fracture surface: (A) frozen-in strain of 50%, and (B) frozen-in strain of 70%. [Color figure can be viewed in the online issue, which is available at wileyonlinelibrary.com.]

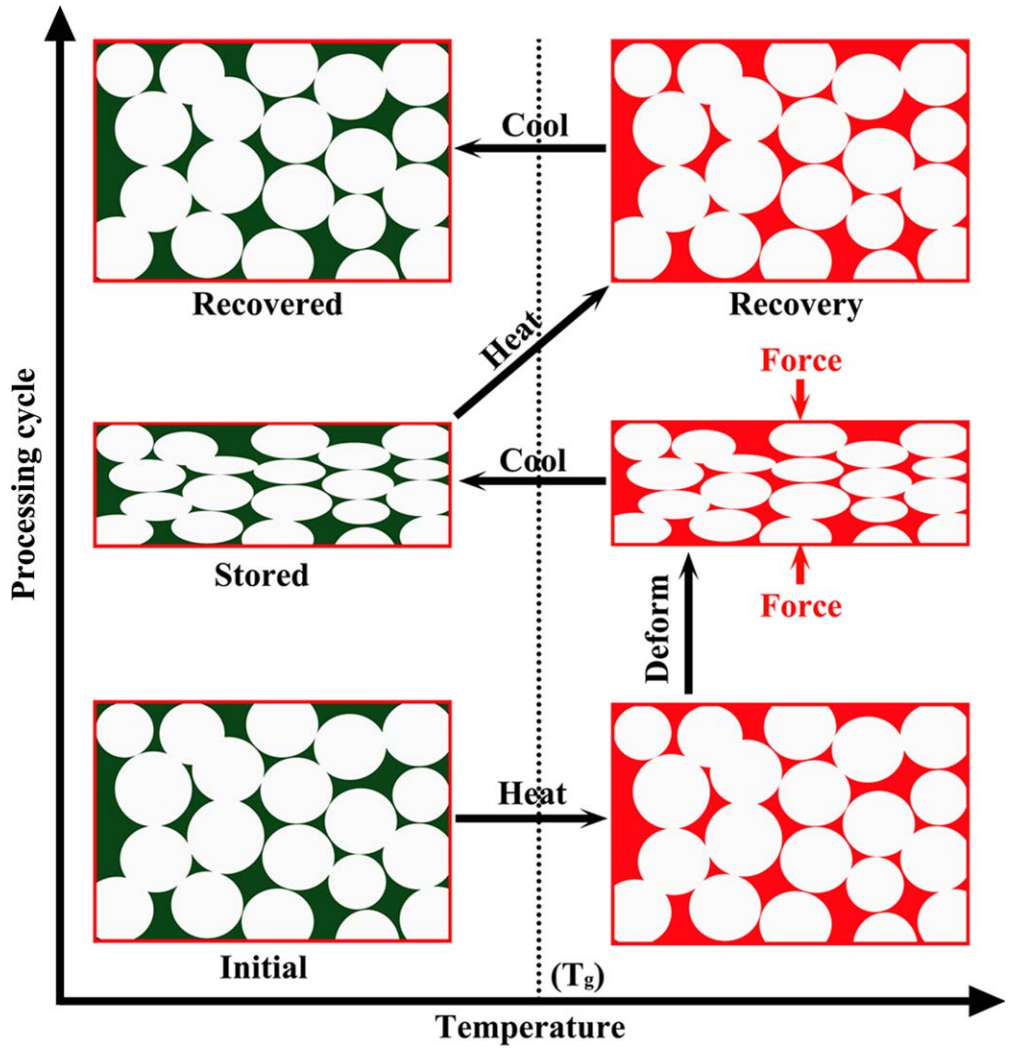

Figure 10. Schematic of the thermo-mechanical deformation and recovery cycle used to investigate the SMP behavior of these materials. [Color figure can be viewed in the online issue, which is available at wileyonlinelibrary.com.]

70% the porous structure became highly flattened, as shown in Figure 9(B). The thermo-mechanical deformation sequence and recovery process are illustrated in Figure 10.

The stress–strain–temperature curve of the silica/WEP foam (SMF2) obtained in the thermo-mechanical cycle test using the maximum strain ($\varepsilon_m = 70\%$) is shown in Figure 11. The stress–strain–temperature curves of the other samples are similar and therefore not shown in present study. The compressive fixity ratio (R_f) and recovery ratio (R_r) over a total of five cycles of the silica/WEP foams are listed in Table II. R_f is defined as the ability of the SM material to maintain its temporary shape after cooling when the applied stress is removed. R_r is the ability of the SM material to recover its initial shape upon heating and measured as the ratio of strain variation during recovery over strain variation during the preceding deformation. R_f and R_r are two important parameters for determining and evaluating SM material characteristics, as defined by eq. (2).[39] The four steps associated with the shape fixity and shape recovery are highlighted. R_f and R_r are determined in terms of the strain, where

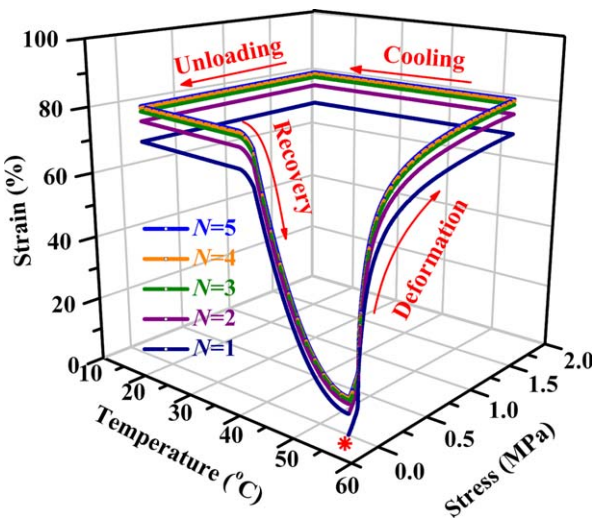

Figure 11. Shape memory properties of the silica/WEP foam SMF2 evaluated by four-step thermo-mechanical cycle. [Color figure can be viewed in the online issue, which is available at wileyonlinelibrary.com.]

Table II. Effect of Thermo-Mechanical Cycle on R_r and R_f

	SMF1		SMF2		SMF3	
N^a	R_r (%)	R_f (%)	R_r (%)	R_f (%)	R_r (%)	R_f (%)
1	91.3	99.7	90.4	99.8	87.5	99.9
2	96.0	99.7	95.8	99.7	95.2	100
3	99.1	99.7	98.5	99.8	96.8	100
4	99.3	99.8	99.2	99.8	98.6	99.9
5	99.6	99.7	99.5	99.7	99.0	100

[a] Thermo-mechanical cycle number.

N is the number of thermo-mechanical cycles ($N = 1$, 2, 3, 4, and 5 in Figure 11), ε_m is the pre-deformation strain (strain at the end of step 2), ε_u is the temporary strain fixed (strain at the end of step 3), and ε_p is the permanent strain (strain at the end of step 4).

$$R_f(N) = \frac{\varepsilon_u(N)}{\varepsilon_m}, \text{ and } R_r(N) = \frac{\varepsilon_m - \varepsilon_p(N)}{\varepsilon_m - \varepsilon_p(N-1)} \quad (2)$$

After the first cycle ($N = 1$), R_r values reached >~87% during the subsequent cycle for all foams. An increase in R_r (>~95%) after the first SM cycle ($N \geq 2$) can be observed in Table II. This phenomenon is called "training" effect:[39] the first SM cycle removes the residual strain that originates from processing such that subsequent shape recovery is improved. R_f was clearly high (~100%) after five thermo-mechanical cycles for all samples.

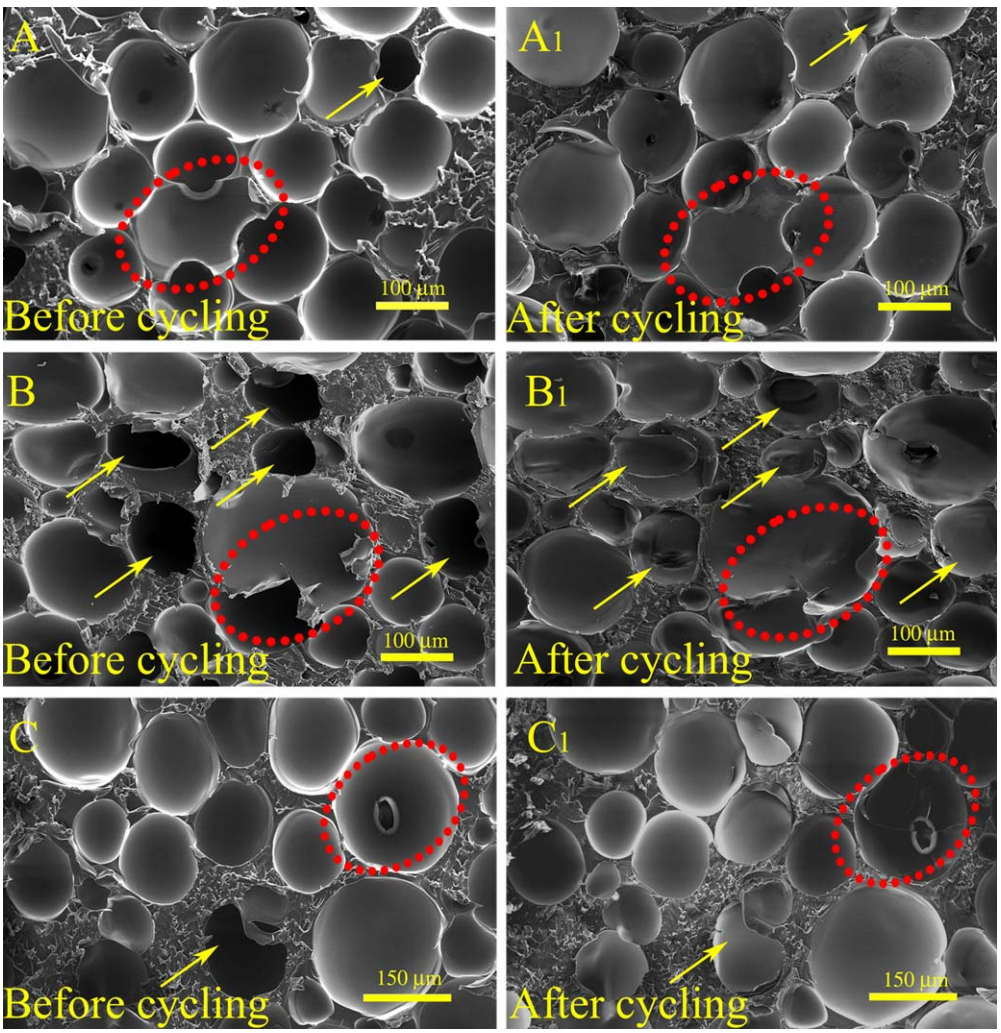

Figure 12. SEM micrographs of foam fracture surfaces following five deformation and recovery cycles: (A and A1) SMF1, (B and B1) SMF2, and (C and C1) SMF3. [Color figure can be viewed in the online issue, which is available at wileyonlinelibrary.com.]

This result suggests that high performance smart materials with excellent SM properties were achieved. The shape fixity ratio of the foams decreased from about 99.9 (SMF3) to 99.7% (SMF1), whereas the shape recovery ratio increased from 87.5 (SMF3) to 91.3% (SMF1) with increasing freeze-drying time. These results indicate that the shape fixity and shape recovery ratio depended on the glassy state and the rubbery state modulus of the foams, respectively.[40] Figure 12 shows the effect of the five thermo-mechanical cycles on the surface morphology of the silica/WEP foams. The foams maintained their original spherical void structures following five cycles. These results suggest that the silica/WEP foam with excellent SM functionality were successfully prepared from WEP via an eco-friendly technology. In addition, some black holes (marked with yellow arrow) were observed in the cross-section of the foams and were filled by the internal cell wall of the foam after the thermal-mechanical cycle, as shown in Figure 12.

CONCLUSIONS

In this study, novel silica/WEP SM composite foams were prepared without adding a foaming agent. The effect of freeze-drying time on the morphological, mechanical, and SM properties of the silica/WEP foams were investigated. When the freeze-drying time increased, the density, cell density, T_g, compression strength and modulus of the foams increased, whereas the size of the cell decreased. The composite foams possessed excellent SM properties. The shape fixity ratio of the foams decreased from 99.9 (SMF3) to 99.7% (SMF1), whereas the shape recovery ratio increased from 87.5 (SMF3) to 91.3% (SMF1) with increasing freeze-drying time. The composite foams could maintain their high shape recovery and fixity ratios at more than 90% even after five thermo-mechanical cycles. In this study, we proposed an environmentally friendly foaming technique (without organic foaming agent) that avoids the risks of safety production and environmental problems, such as workers' health, flammability, ozone depletion, and global warming. Moreover, this work contributes to the field of WEP composite foam with SM property. Further developments are in progress and mainly focused on obtaining composite foams with excellent SM properties, along with satisfactory mechanical properties.

ACKNOWLEDGMENTS

This work was supported by the National Natural Science Foundation of China (NSFC) (Grant No.51473147).

REFERENCES

1. Lu, H.; Zhu, S.; Yang, Y.; Huang, W. M.; Leng, J.; Du, S. *J. Appl. Polym. Sci.* **2015**, *132*, 41673.
2. Luo, H.; Hu, J.; Zhu, Y.; Wu, J. Y.; Zhang, S.; Fan, Y.; Ye, G. *J. Appl. Polym. Sci.* **2013**, *127*, 675.
3. Cai, Y.; Feng, X.; Jiang, J. S. *J. Appl. Polym. Sci.* **2014**, *131*, 40220.
4. Ding, J.; Zhu, Y. F.; Fu, Y. Q. *Polym. Composite.* **2014**, *35*, 412.
5. Kang, H.; Li, M.; Tang, Z.; Xue, J.; Hu, X.; Zhang, L.; Guo, B. *J. Mater. Chem. B* **2014**, *2*, 7877.
6. Dong, Y.; Ni, Q. Q.; Fu, Y. *Compos. Part A* **2015**, *72*, 1.
7. Ma, M.; Guo, L.; Anderson, D. G.; Langer, R. *Science* **2013**, *339*, 186.
8. Chen, H.; Li, Y.; Liu, Y.; Gong, T.; Wang, L.; Zhou, S. *Polym. Chem.* **2014**, *5*, 5168.
9. Lendlein, A.; Jiang, H.; Junger, O.; Langer, R. *Nature* **2005**, *434*, 879.
10. Cai, Y.; Jiang, J. S.; Zheng, B.; Xie, M. R. *J. Appl. Polym. Sci.* **2013**, *127*, 49.
11. Wang, W.; Liu, D.; Liu, Y.; Leng, J.; Bhattacharyya, D. *Compos. Sci. Technol.* **2015**, *106*, 20.
12. Lee, S. H.; Jung, J. H.; Oh, I. K. *Small* **2014**, *10*, 3880.
13. Cai, Y.; Jiang, J. S.; Liu, Z. W.; Zeng, Y.; Zhang, W. G. *Compos. Part A* **2013**, *53*, 16.
14. Singhal, P.; Small, W.; Elizabeth, C. H.; Maitland, D. J.; Wilson, T. S. *Acta Biomater.* **2014**, *10*, 67.
15. Fabrizio, Q.; Loredana, S.; Anna, S. E. *Mater. Lett.* **2012**, *20*, 20.
16. Li, G.; Uppu, N. *Compos. Sci. Technol.* **2010**, *70*, 1419.
17. Chung, S. E.; Park, C. H. *J. Appl. Polym. Sci.* **2010**, *117*, 2265.
18. Kang, S. M.; Lee, S. J.; Kim, B. K. *Express. Polym. Lett.* **2012**, *6*, 63.
19. Li, G.; John, M. *Compos. Sci. Technol.* **2008**, *68*, 3337.
20. Li, G. Q. Nettles, D. *Polymer* **2010**, *51*,755.
21. Rousseau, I.; A. Xie, T. *J. Mater. Chem.* **2010**, *20*, 3431.
22. Prima, M. D.; Gall, K.; Mcdowell, D. L.; Guldberg, R.; Lin, A.; Sandderson, T.; Campbell, D.; Arzberger, S. C. *Mech. Mater.* **2010**, *42*, 304.
23. Squeo, E. A.; Quadrini, F. *Smart. Mater. Struct.* **2010**, *19*, 105002.
24. Wang, L.; Yang, X.; Jiang, T.; Zhang, C.; He, L. *J. Appl. Polym. Sci.* **2014**, *131*, 41175.
25. Wang, L.; Yang, X.; Zhang, J.; Zhang, C.; He, L. *Compos. Part B* **2014**, *56*, 724.
26. Xie, P.; Liu, H.; Qiu, S. J.; Rong, M. Z.; Zhang, M. Q.; Lu, Z. Y.; Wu, S. P. *Green Chem.* **2014**, *16*, 1225.
27. Chen, L.; Goren, B. K.; Ozisik, R.; Schadler, L. S. *Compos. Sci. Technol.* **2012**, *72*, 190.
28. Dong, Y.; Ni, Q. Q.; Li, L.; Fu, Y. *Mater. Lett.* **2014**, *132*, 206.
29. Tang, Z.; Sun, D.; Yang, D.; Guo, B.; Zhang, L.; Jia, D. *Compos. Sci. Technol.* **2013**, *75*, 15.
30. Han, S.; Chun, B. C. *Compos. Part A* **2014**, *58*, 65.
31. Zhang, Y.; Wang, Q.; Wang, C.; Wang, T. *J. Mater. Chem.* **2011**, *21*, 9073.
32. Lee, S. K.; Yoon, S. H.; Chung, I.; Hartwig, A.; Kim, B. K. *J. Pol. Sci. Pol. Chem.* **2011**, *49*, 634.
33. Dong, Y.; Wang, R.; Li, S.; Yang, H.; Du, M.; Fu, Y. *J. Colloid Interf. Sci.* **2013**, *391*, 8.
34. Wegmann, A. *Prog. Org. Coat.* **1997**, *32*, 231.

35. Dong, Y.; Ni, Q. Q. *Polym. Composite.*, to appear. DOI: 10.1002/pc.23082.
36. Leng, J.; Wu, X.; Liu, Y. *Smart Mater. Struct.* **2009**, *18*, 95031.
37. Behl, M.; Bellin, I.; Kelch, S.; Wagermaier, W.; Lendlein, A. *Adv. Funct. Mater.* **2009**, *19*, 102.
38. Small, W.; Singhal, P.; Wilson, T. S.; Maitland, D. J. *J. Mater. Chem.* **2010**, *20*, 3356.
39. Ni, Q. Q.; Zhang, C. S.; Fu, Y.; Dai, G.; Kimura, T. *Compos. Struct.* **2007**, *81*, 176.
40. Smela, E. *Adv. Mater.* **2003**, *15*, 481.